# Evolution of Nuclear Collectivity at High Spins and Temperatures

CONF-8908129--6

DE92 004220

C. Baktash

*Physics Division, Oak Ridge National Laboratory, Oak Ridge, TN 37831-6371, USA*

## 1. Introduction

Atomic nuclei provide a unique laboratory for the study of quantal systems under the extreme conditions of high temperature, spin, isospin, as well as baryonic and energy densities. In the past few years, we have witnessed a rapid progress toward understanding the properties of *cold* rapidly-rotating nuclei. For example, the spectroscopy of the discrete superdeformed, as well as normally-deformed states in the 50–60 $\hbar$ spin range is becoming "routine", thanks to both the ingenuity of the experimentalists, and the advent of powerful gamma-ray detection systems. These technical feats have been similarly matched, or oftentimes surpassed, by the impressive achievements in the theoretical understanding of the nuclear behavior at high spins. After all, theoretical calculations predicting the presence of superdeformed states at high spins preceded the discovery of these states by almost a decade.

The picture, unfortunately, is not as bright when it comes to the understanding of the nuclear properties at finite temperature which, both theoretically and experimentally, remain rather limited. This lack of knowledge, however, is not due to the want of interesting physics to be addressed in this regime. Quite on the contrary, dramatic structural changes are expected to unfold as the excitation energy is increased. The spin-temperature map of Fig. 1 shows a schematic phase diagram of nuclei at finite temperature. Gradual vanishing of the pairing correlations, onset of chaos, prolate-to-oblate shape changes, melting of the shell effects, and eventually the inability of the compound nucleus (CN) to sustain giant resonances at very high temperatures ( "death" of CN ) are only a few examples of the rich and varied phenomena yet to be explored. Equally important is the question of thermal fluctuations and the extent to which they modify the above phase transitions.

Heavy-ion fusion-evaporation reactions remain the basic tool to form and study hot nuclei. Unfortunately, many important parameters that influence, or even determine the formation and decay of compound nuclei are not yet reliably known. Among these are the evolution with spin and temperature of the level density, gamma-ray strength functions and transmission coefficients. These parameters determine the competition between neutron, charged-particle, and gamma emission and, thus, critically enter into our Monte Carlo simulations of the CN decay, upon which interpretations of the bulk of the experimental data rest. Naturally, a vigorous theoretical and experimental undertaking must be attempted to remedy the

situation before we can fully explore the various phases of nuclear matter at finite temperature that was outlined above.

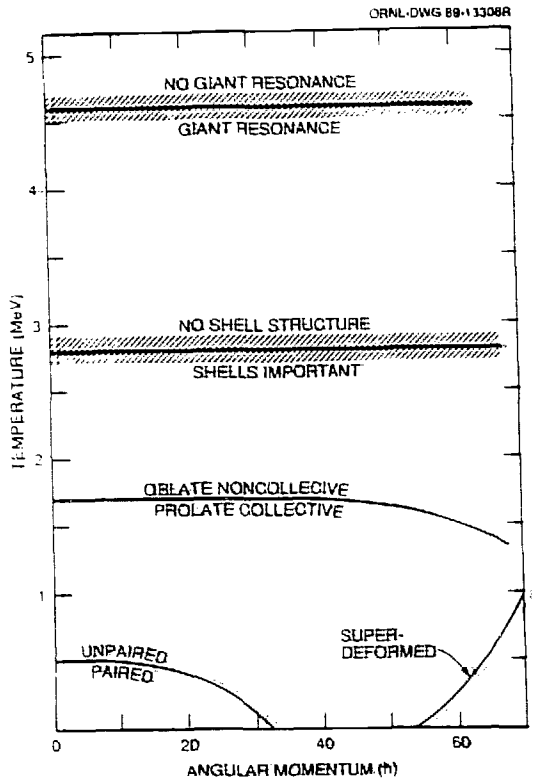


Fig. 1 A temperature vs. spin map showing a schematic phase diagram of nuclei at finite temperature.

Until recently, experimental techniques did not lend themselves well to the task of isolating temperature and spin effects. To go to higher spins or temperatures, one would raise either the beam energy or select a higher total-gamma energy cut. This, however, would raise *both* the spin and temperature of the system, thus making it difficult to identify the origin of the observed changes. This problem has been solved by devising the so called Crystal Balls, $4\pi$ gamma-detection systems that simultaneously register both the total coincidence gamma-ray energy ($H$), and the fold ($k$) on an event-by-event basis. These two parameters are proportional to the excitation energy ($E$), and spin ($I$) of the entry states, respectively. The Spin Spectrometer[1] at ORNL is one such device which consists of 72 NaI detectors to provide for $4\pi$ coverage.

In the past few years, we have utilized the Spin Spectrometer and a variety of complementary probes (continuum $\gamma$ rays, proton- $\gamma$ coincidence spectroscopy and $\gamma$ decay of GDR) to study the the nuclear response to the *DIFFERENTIAL* effects of increasing spin and temperature for constant values of excitation energy or spin,

respectively. In the following sections we shall describe two of these experiments that trace the properties of rapidly-rotating nuclei at small to moderate excitation energies.

## 2. Continuum $E2$ and $M1$ Transitions as a Probe of Shapes at Moderate Temperatures

For these studies we chose the nucleus $^{158}$Yb which, due to its transitional nature, readily responds to the shape-driving forces. From our earlier spectroscopic studies[2] , it has been established that this nucleus experiences band termination[3], and undergoes a prolate-to-oblate shape transition along its yrast line at a spin of $\approx 36\hbar$.

The high-spin states in $^{158}$Yb were populated via the $^{98}Mo(^{64}Ni, 4n)$ reaction at 285-MeV beam energy. The experimental setup consisted of six Ge detectors places in the Spin Spectrometer as described in Ref. 2. All of the energy and timing information of the NaI- and Ge-detectors were recorded event by event on tape. After matching the gains of all NaI detectors, and removing pulses due to neutrons, a series of NaI spectra were generated subject to the following gates: (1) discrete $\gamma$ rays that deexcite states with $I^{\pi} = 2^{+}$–$12^{+}$ in $^{158}$Yb for channel selection; (2) total coincidence fold ($k$) in steps of $\Delta k = 1$; (3) total pulse height $H$ in steps of $\Delta H = 1.6MeV$; and (4) polar angles of the NaI detectors. The resulting 2048 spectra were then unfolded and relabeled by their corresponding total multiplicity ($M$) and excitation energy ($E$). For each distinct set of $(E, M)$ gate-value, the unfolded spectra were sliced into bins of 100 keV and the angular distribution of the intensity in each bin was fitted to the expression $W(\theta) = A_0[1 + a_2P_2(cos\theta) + a_4P_4(cos\theta)]$. Using the fitted values of the $a_2(E_\gamma)$ and $a_4$ $(E\gamma)$ coefficients, we were able to decompose the energy spectra into two spectra of dipole and qudrupole $\gamma$ rays.

The four panels in Fig. 2 show the evolution of the quadrupole (solid curves) and dipole (dashed curves) multipolarity spectra with increasing spin (left to right) and excitation energy (bottom to top) at constant $E^*$ and $I$ ,respectively ($E^*$ denotes the excitation energy above the yeast line). The quadrupole $\gamma$-ray spectra show two distinct structures. First, there exists a strong and narrow peak around $E_\gamma \approx$750 keV which is rather stable with increasing $I$ and $E^*$. Nearly 60% of this peak is due to the deexcitation of the yrast states in the $I \approx$26–36$\hbar$, while the remaining strength originates from the "quasivibrational" continuum transitions at higher $E^*$, whose transition energies slowly decrease with increasing excitation energy. While the high-energy edge of this peak falls rapidly, a second and much broader quadrupole structure gradually develops around 1.15 MeV. From Fig. 2 it is apparent that the intensity of this structure grows with increasing excitation energy and persists upto about $E^* \approx$10 MeV. In the backed-target experiment, comparisons of the spectra at angles of $\theta = +24°$ and $\theta = -24°$ indicate that this structure is fully Doppler shifted. Since the stopping time of the recoiling nuclei in the lead backing of the target is of the order of 1 ps, this observation implies that these transitions are collective. That

is, at sufficiently high spins, the nucleons undergoes a noncollective-to-collective transition with increasing excitation energy.

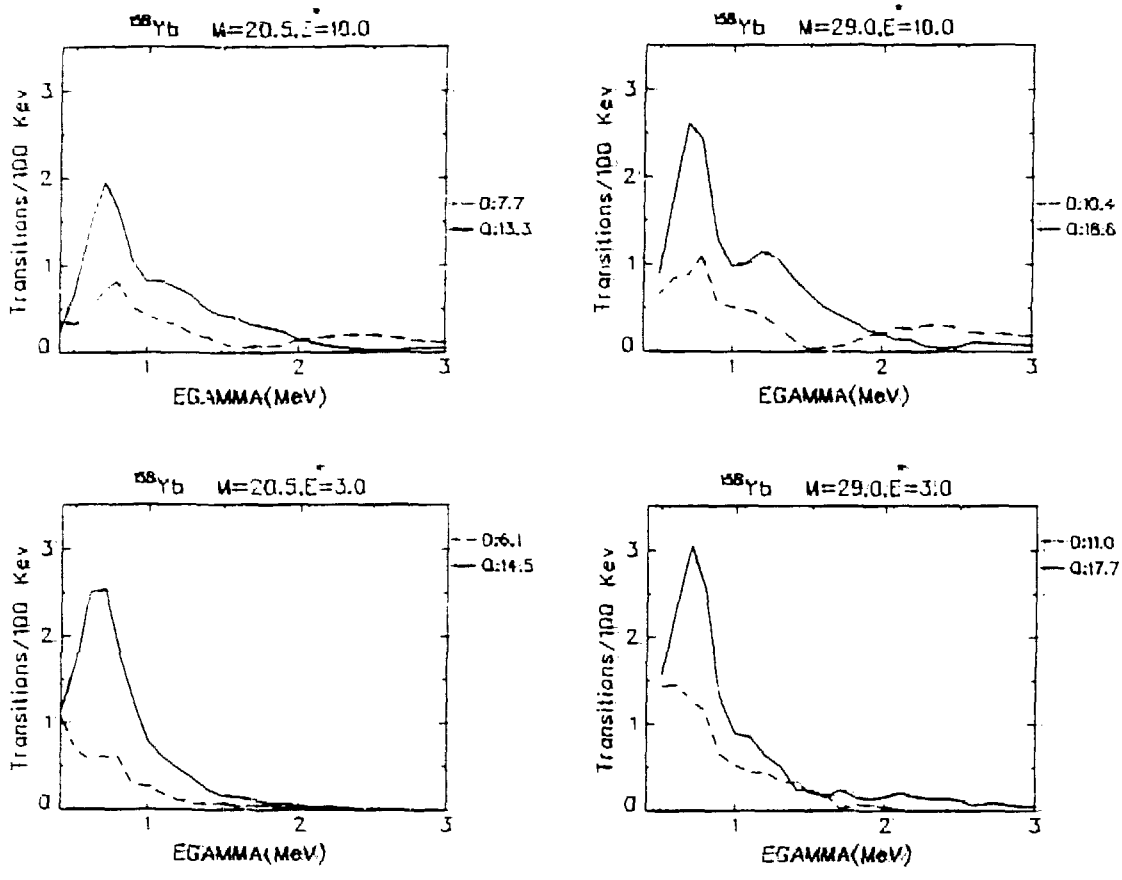


Fig. 2 Evolution of the qudrupole (solid lines) and dipole (dashed lines) spectra with excitation energy ($E^*$) and multiplicity ($M$). Each panel is labeled with the corresponding values of $E^*$ and $M$. Noteworthy structures that become strong at high multiplicities are: A qudrupole bump ($E_\gamma \approx$1.15 MeV); and a broad dipole structure ($E_\gamma \approx$1.5–3 MeV) at high $E^*$; and a low-energy continuum dipole at low $E^*$

The dipole-like $\gamma$-ray spectra also show two distinct features. First, at energies of less than $\approx$750 keV, we observe a continuum of $\gamma$ rays whose intensity grows with increasing multiplicity, but diminishes with $E^*$. This clearly identifies the near-yrast high-spin states as their origin. In contrast, a very broad structure, with a centroid at about 2.5 MeV, develops at high spins and excitation energies as seen in Fig. 2.

To ascertain the $EM$ character of the dipole-like transitions, the angular distribution data were analyzed in terms of two limiting cases, namely: (1) quadrupole plus *mixed stretched* ($\Delta I = 1$) transitions, or (2) quadrupole plus *mixed unstretched*

($\Delta I = 0$) transitions. A fit to the data indicates that the low-energy part of the spectrum ($E_\gamma < 1$ MeV) favors the first solution, whereas the high-energy part of the spectrum ($E_\gamma > 2$ MeV) is best reproduced by the second solution. The deduced mixing ratios fall in the range of 1.5–3 and 1–1.5 for the two solutions, respectively. Such large mixing ratios rule out an $M2$, $E1$ character for the dipole-like transitions. A further evidence in support of the $M1$ character of these gamma rays comes from the fact that they,too, are fully Doppler shifted, indicating a $B(M1) \approx 1$ W.U. Evidence for the presence of intense low-energy $M1$ transitions at high spins has been reported by Janssens *et al.*[4] in $^{153}$Ho.

Taken together, these observations point to the existence of two very different structures at high spins in $^{158}$Yb nucleus. In the vicinity of the yrast line, the presence of the low-energy mixed $E2/M1$ transitions rather than high-energy $E2$ transitions indicates that these states are only weakly collective. Possible candidate structures are: (1) weakly-collective triaxial bands, or (2) terminating bands similar to those observed at lower spins ($I \approx 40$) in the discrete-spectroscopy data[2]. (In the band-termination regime, the reduced $E2$ strength allows the $M1$ transitions to be competitive.) In contrast, at high-excitation energies, the presence of collectively-enhanced $E2$ transitions at $E_\gamma \approx 1.15$ MeV, and the $M1$ $\gamma$ rays with $E_\gamma \approx$2–3 MeV signal the onset of collectivity well *above* the yrast line.

It is worth mentioning that double-humped continuum structures have been previously observed in several of the $N \approx 86$ nuclei[5–9]. However, while the higher energy component ($E_\gamma \approx$1200 keV) has been correctly identified as a collective $E2$ structure, the lower bump at $E_\gamma \approx$750 keV was misidentified to be predominantly of $M1$ character in Refs. 6–9. Consequently, these authors have attributed these bumps to high-K rotational bands which give rise to $M1$ transitions at half the energy of the $E2$ gamma-rays. The present study reveals that, first, the strong peak at 750 keV is predominantly of $E2$ character. Secondly, the low-energy continuum $M1$ gamma-rays in Fig. 2 are *anticorrelated* with the high-energy collective qudrupole bump. That is, they originate from regions of widely different excitation energy.

Of particular interest is the high-energy $M1$ component which provides a powerful probe of nuclear collectivity at high temperatures. As previously shown by Chen and Hamamoto[10], as well as by Chen and Leander[11], for rotational bands with large deformation and moderate values of K, $M1$ transitions can effectively compete with the intraband collective $E2$ transitions. Furthermore, the centroid of the $M1$ structure is a very sensitive indicator of the deformation parameter $\epsilon_2$, and increases almost linearly with it. These predictions are borne out in the present data. Figure 3 compares the observed $M1$ and $E2$ spectra with their respective probability distributions from a cranked shell model calculation. Similar to the experimental data, the strength of the calculated $M1$ bump increase with increasing temperature. A deformation parameter of $\epsilon_2$=0.36 is needed to reproduce the experimental centroid of the $M1$ structure. For comparison, a smaller value of $\epsilon_2$=0.16 results in a centroid energy of 1.5 MeV. The above deduced deformation is in excellent accord with the results of calculations by Dudek and Nazarewicz[12] which

predict a transition from noncollective back to well-deformed collective structures at high spins and excitation energies in $^{158}$Yb. The collective features observed in this experiment persist upto one-neutron binding energy and clearly establish that *shell effects survive and dominate the structure of warm, rapidly-rotating nuclei in this region.*

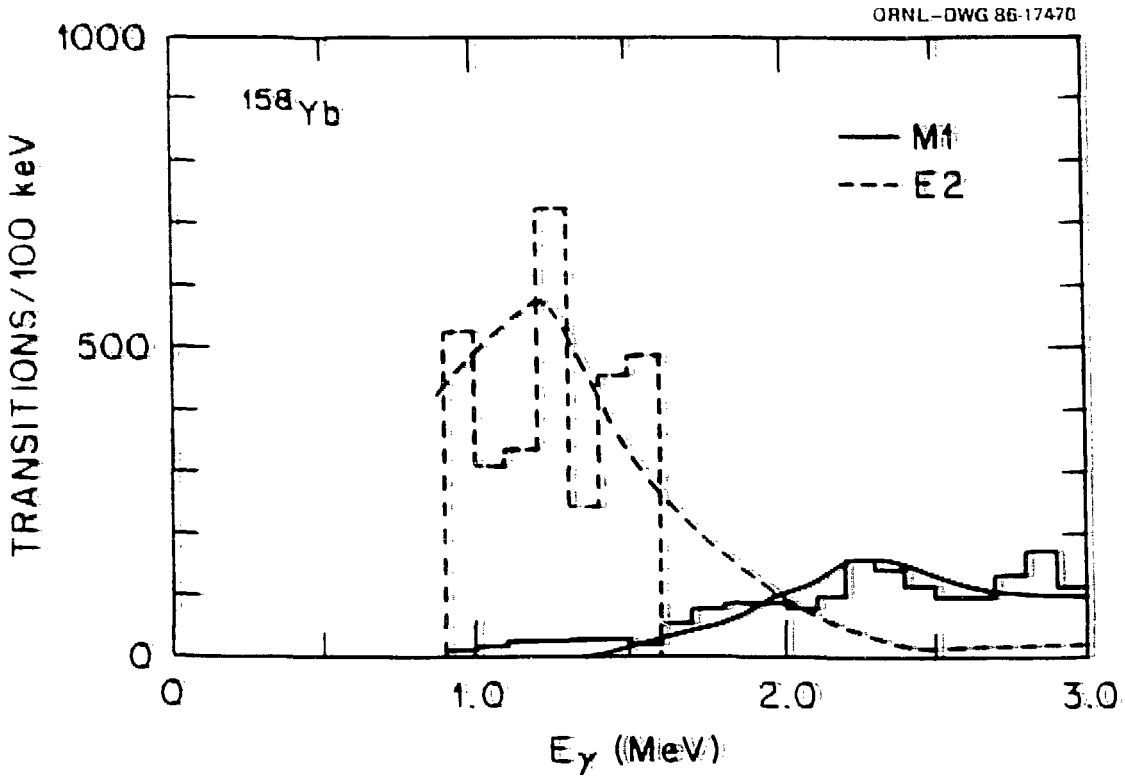


Fig. 3 The probability spectra of $M1$ (solid line) and $E2$ (dashed line) for $^{158}$Yb calculated with parameter $\epsilon_2$=0.36, $\epsilon_4$=-0.015, and $\gamma$=0. They are generated by summing over the contributions from the N=5,6 neutron, and N=5 proton shells for rotational frequencies that correspond to a spin range of I=30-55$\hbar$. All quasiparticle levels within 9 MeV above the yrast line are included in the calculation. The smooth solid and dashed curves are the experimental $M1$ and $E2$ spectra, respectively. The y-axis scale is arbitrary.

Recent finite-temperature HFB cranking (FTHFBC) calculations [13] predict a prolate to noncollective oblate transition in $^{158}$Yb above the critical spin of $\approx 40\hbar$, where a flat $\gamma$-soft potential-energy surface persists at all excitation energies. However, at higher $E^*$, thermal fluctuations give rise to a modest *dynamic* qudrupole deformation ($\epsilon_2 \approx 0.1$) and collectivity ($B(E2) \approx 100$ W.U.)[14]. While these calculations produce qualitative features of the data, quantitative agreement is lacking. Specifically, if fluctuations alone were responsible for the observed collectivity at high

excitation energies, then the associated high-energy $M1$ transitions would be distributed over a large energy region. To reproduce a distinct continuum high-energy $M1$ structure, a well-defined minimum in the potential-energy surface is called for. Inclusion of the high-j intruder orbitals from the higher-lying shells which are left out of the present calculations would increase $\epsilon_2$ and, hence, will be a step in the right direction. At lower spins, the theory correctly reproduces the boundary where the transition energies change from a quasivibrational to a quasirotational pattern.[15]

In another self-consistent FTHFBC calculation, Egido and Weidenmüller have studied the variation of the $\gamma$-strength functions with spin and temperature.[16] In sharp departure from the simple forms used in the statistical models, their results display sizable (several orders of magnitude) fluctuations in the matrix elements of the noncollective transitions. Even more interesting is their finding that the calculated $E1/M1$ ratios vary with the gamma-ray energy, and favor magnetic emission for $E_\gamma < 3$ MeV. (In the conventional statistical models, this ratio is a straight horizontal line and normally favors the $E1$ statistical emission.) Similarly, at a temperature of $T \approx 0.7$ MeV, the magnetic transitions can even favorably compete with the $E2$ transitions for certain $\gamma$-ray energies. The enhanced $M1$ transition at high excitation energies observed in our experiment is in good accord with these findings.

These results establish a clear need for a detailed study of the $\gamma$-ray strength fuctions at finite temperatures in general, and the role of magnetic transitions in particular. Inasmuch as these parameters critically enter into our simulations of the statistical cooling of the CN, decay pathways, and rotational damping, one should take their possible variation into account when relying on the statistical models to interpret the experimental data.

## 3. Nuclear Structure Effects in Proton Evaporation Spectra

It has been known for some time that $\alpha$-particle emission from excited nuclei , particularly below the evaporation Coulomb barrier, is sensitive to nuclear shapes.[17–21] Previous work has demonstrated that a decrease in the evaporation barrier for $\alpha$-particles due to deformation is capable of explaining $\alpha - \gamma$ angular distribution data[19–21] and $\alpha$-particle energy spectra.[22] In earlier work employing heavy-ion fusion reactions, such data were obtained with small particle-detection efficiency, and either without exit channel-selection or by gating on $\gamma$-ray multiplicity which provided some channel selection. In the present work we have taken a major step forward by combining exit channel selection with $4\pi$ detection of the charged particles, and $4\pi$ detection of the $\gamma$ rays. This allowed us to obtain proton spectra with very good statistics in coincidence with many specific transitions in each rotational band in the final nucleus, and to study their shapes as a function of the spin of the entry states in the same final nucleus.

We have chosen to study $^{82}$Sr as the final nucleus because it was predicted to have a superdeformed band structure at high spins.[23] The experiment was performed using the $^{52}$Cr($^{34}$S, 2p2n)$^{82}$Sr reaction at 130 MeV. The discrete $\gamma$ rays from the evaporation residues were detected with 18 Compton-suppressed Ge detectors

inserted in the Spin Spectrometer. The light-charged particles (protons, deuterons, $^3$He and $\alpha$-particles) were detected with the Dwarf Ball,[24] a $4\pi$ array of 72 CsI(T$\ell$) detectors. The event-trigger condition was that two or more Ge detectors and one or more CsI(T$\ell$) detectors fire in coincidence. Particle identification was accomplished by pulse-shape discrimination with the CsI(T$\ell$) pulses. The particle energies were converted event by event to the center-of-mass system, assuming compound nucleus formation and decay to one proton. This allowed total spectra and angular distributions in the center-of-mass system to be obtained by appropriate summing of spectra from the Dwarf Ball detectors. For charged-particle channel selection, all the Dwarf Ball detectors were used, but for energy spectra the detectors at $\theta_{lab}$ of 24°, 42°, 50°, 63°, 68°, 78°, 87°, 93° and 102° were employed.

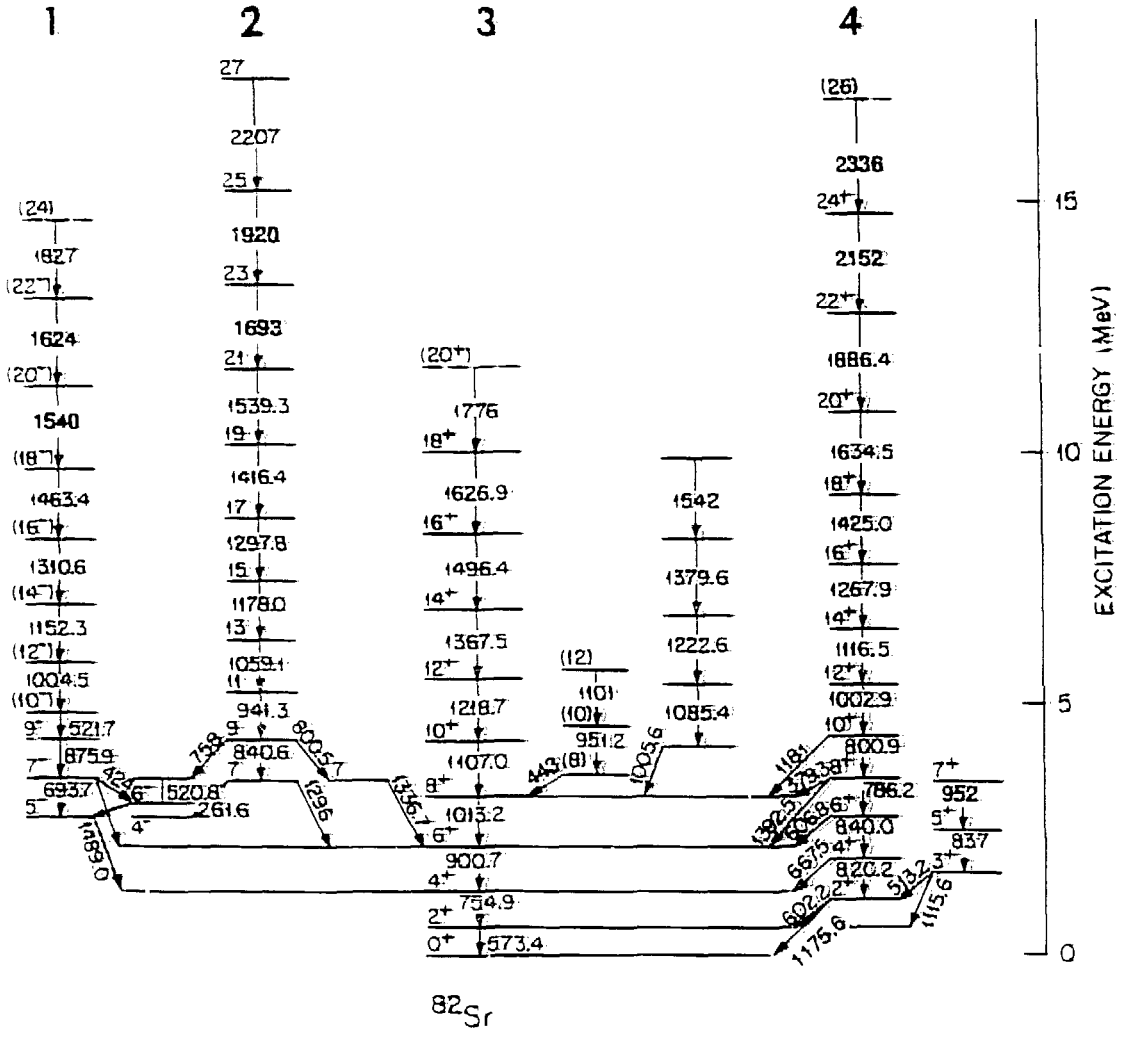


Fig. 4 Partial level scheme for $^{82}$Sr showing four major rotational bands. Band 3 is the ground band, and band 4 is the yrast one. The odd spin band 2 becomes yrast at spins higher than 23.

Figure 4 shows a new level scheme for $^{82}$Sr obtained in this work[25]. In the level scheme, band 4 is yrast for spins between 10 and 22 $\hbar$, while the odd-spin band 2 becomes yrast for I > 23. Proton spectra coincident with the $2^+ \rightarrow 0^+$ ground transition are shown in Fig. 5(a) for the three $k_\gamma$ gates. For the higher $k_\gamma$ gates the proton spectra shift to lower energies and become narrower, but the high energy slopes (above ~15 MeV) for all the $k_\gamma$ gates are similar. This behavior is understood in terms of the decreasing thermal energy as $k_\gamma$ or equivalently the spins of the entry region are increased (the three $k_\gamma$ gates correspond to I ~ 4-19, 17-29 and 26-45 $\hbar$, and to average yrast energies of 7, 14, and 23 MeV, respectively). A statistical-model calculation with the evaporation code PACE[20] for this system reproduces these features at least qualitatively. This is shown in Fig. 5(b).

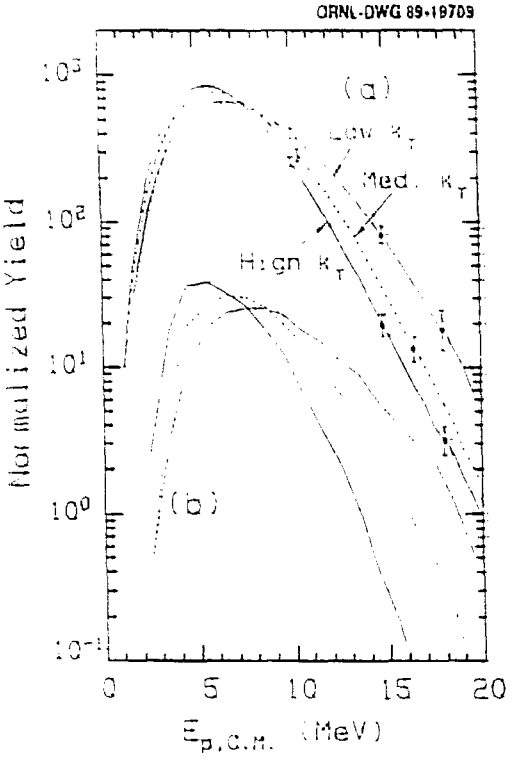


Fig. 5 (a) Proton spectra coincident with the $2^+ \rightarrow 0^+$ transition in the ground band (band 3 in Fig. 4) of $^{82}$Sr for the three $k_\gamma$ gates indicated. The spectra are normalized to the same area for comparison (the peak counts/0.5 MeV are 8036±135, 25025±213, and 15369±171, respectively). Typical statistical error bars are shown for selected bins. (b) Normalized theoretical proton spectra calculated with the evaporation code PACE for the three $\gamma$-ray multiplicity gates corresponding approximately to the $k_\gamma$ bins in (a).

In order to explore any dependence of the proton emission probability on the structure of the final nucleus, we have compared the shapes of the proton spectra coincident with $\gamma$-rays from levels of increasing spin in each rotational band and of the same spin in different rotational bands. The $2^+$, $4^+$ and $6^+$ levels in the ground band (band 3 in Fig. 4) are populated strongly from all the bands in $^{82}$Sr. Therefore, the proton spectra generated by gating on $\gamma$-rays from these levels should be very similar to each other. This is indeed seen to be the case in Fig. 6(a). For spins higher than 8 $\hbar$ the observed $\gamma$ decay stays within a given rotational band (Fig. 4). Therefore any dependence of the shape of the proton spectrum on structure should become apparent only for spins 10 or higher.

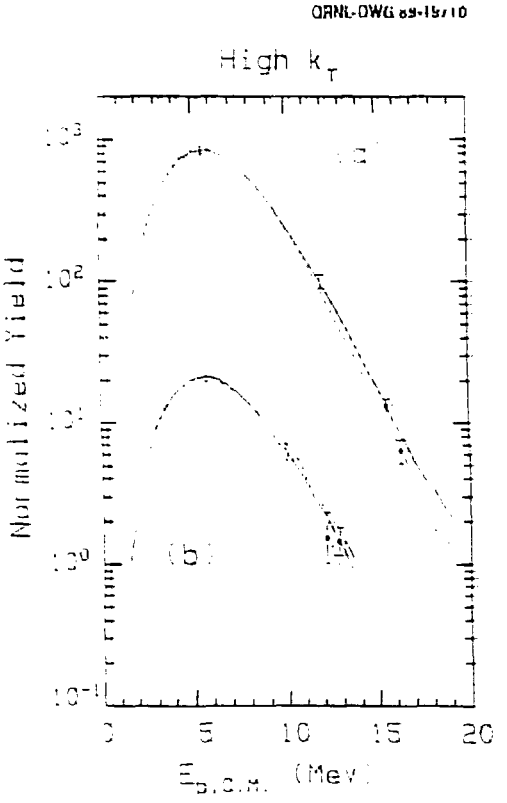


Fig. 6 (a) Proton spectra coincident with transitions from the $2^+$, $4^+$, and $6^+$ levels of the ground band in $^{82}$Sr for the high $k_\tau$ gate (thin, thick, and dashed lines, with peak counts/0.5 MeV of 15369$\pm$171, 9620$\pm$130, and 6401$\pm$109, respectively). (b) Proton spectra associated with levels of spin 11, 13 and (19+23) in the odd spin band (band 2) in $^{82}$Sr for the high $k_\tau$ gate (thin, thick, and dashed lines, with peak counts/0.5 MeV of 2003$\pm$83, 1874$\pm$85, and 838$\pm$81, respectively). The spectra in (a) and (b) were normalized to the same area.

Next we examine the proton spectra associated with high spin levels in the same rotational band. Figure 6(b) shows the proton spectra associated with levels of spin 11, 13, and (19–23) in the odd spin band 2 of $^{82}$Sr. Again the spectra are essentially identical in shape.

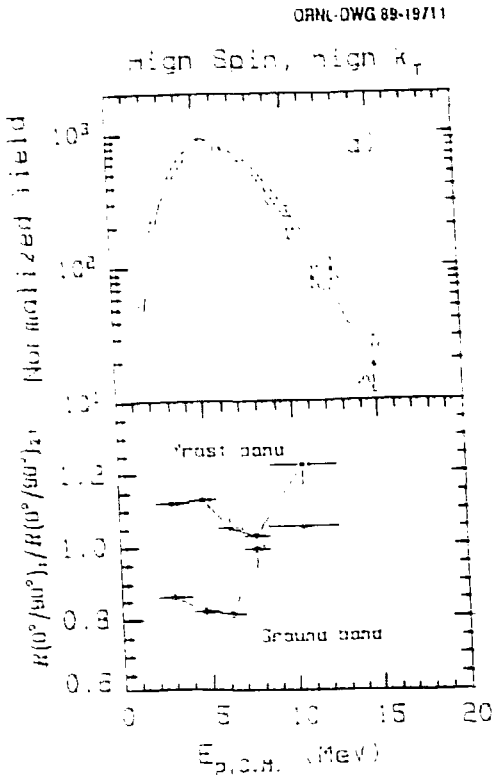


Fig. 7 (a) Proton spectra coincident with the discrete transitions from the ($10^+$ + $14^+$) levels of the ground band 3 (thin line), the spin 13 level of the odd spin band 2 (dashed line), and the ($14^+$ + $16^+$) levels of the yrast band 4 (thick line) for the high $k_\gamma$ gate. The normalized spectra had 1874±85, 1999±97, and 3140±111 counts/0.5 MeV at the peak, respectively. (b) Ratio of the anisotropies of the protons for the high spin levels of the ground band 2 (open squares and thin line) and of the yrast band 4 (closed squares and thick line) relative to the $2^+ \rightarrow 0^+$ ground state transition for the high $k_\gamma$ gate. Vertical bars give statistical errors and horizontal ones the energy bins used for the angular distributions.

In contrast, when we compare proton spectra associated with high spin levels ($\geq 10\hbar$) at comparable excitation energies, large differences are found for all three $k_\gamma$ gates. This is clearly seen in Fig. 7(a), where proton spectra associated with the sum of the $10^+$ and $14^+$ levels in the ground band 3 (thin line), the I=13 level of band 2 (dashed line), and the sum of the $14^+$ and $16^+$ levels of the yrast band 4 (thick line) are shown from the high $k_\gamma$ gate. The striking feature in these spectra is

that for the same $k_\gamma$ gate, the peak of the proton spectrum shifts down by 1 MeV in going from the band 3 to band 2 and then to the yrast band 4. This is comparable in magnitude to the shifts seen in Fig. 5(a) for the $2^- \rightarrow 0^-$ transition from the low to the high $k_\gamma$ gate.

These results are surprising since the entry states are expected to lie at considerably higher excitation energies than the gating transitions and any correlation between the proton spectrum and the nature of the band being populated ought to be washed out by the statistical gamma emission. In fact, somewhat higher thermal energy is available for the yrast band 4 and this should shift its associated proton spectrum in the opposite direction. A possible explanation might be that although we have the same $k_\gamma$ gate, the yrast band is populated from entry regions of higher spins compared to the ground or the other bands. This could cause a shift analogous to that in Fig. 5(a).

We can offer a strong argument against the latter simple explanation in terms of phase-space effects. We note that the energy shifts are comparable to those for the $2^- \rightarrow 0^-$ transition in Fig. 5(a), where the spins and excitation energies for the three $k_\gamma$ gates are greatly different. Consequently, a comparably large difference in the entry regions of the gating transitions should be easily observed experimentally by projecting the actual $k_\gamma$ distributions coincident with the same discrete high spin transitions. We found that the $k_\gamma$ distributions associated with the high spin discrete $\gamma$ gates in the four bands are identical (the average $k_\gamma$ values for the ground, odd spin, and yrast bands were found to be $15.5\pm0.2$, $15.5\pm0.2$ and $15.4\pm0.2$, respectively). In addition, a statistical model calculation in which the high multiplicity gate was moved up by one unit produced a considerably smaller shift in the proton spectrum than observed in Fig. 7(a).

A reasonable explanation for the observed large shifts in the proton spectra is suggested by the steep experimental yrast line and consequently the entry line in $^{82}$Sr and the energy balance in this reaction which places the entry line only a few MeV above the yrast line. This is also confirmed by statistical model calculations. These observations and the data suggest that a significant fraction of the population of the rotational bands in $^{82}$Sr, and in particular the yrast band, occurs by direct proton emission from near-yrast to near-yrast states with the second proton playing that role. This mechanism could explain many features of the data and would in addition require that the last proton emission be streched in character, particularly at and below the emission barrier, where it should exhibit a stronger anisotropy $R(0°/90°) \equiv W(0°)/W(90°)$ with respect to the beam direction. This is indeed what we observe in Fig. 7(b) where the anisotropy ratios for the high spin gates of Fig 7(a) of the ground and the yrast bands are plotted relative to the anisotropy of the $2^- \rightarrow 0^-$ ground transition as a function of the proton center-of-mass energy for the high $k_\gamma$ gate. This further supports this explanation, since the direct population of the ground band has a higher Coulomb barrier compared to that for the population of the yrast band.

Proton emission from the near-yrast states may be associated with a predicted mechanism based on instability toward nucleon emission at large spins, connected with the population of $h_{11/2}$ resonance states in nuclei in this region.[27] These predicted yrast proton transitions were expected to have enhanced anisotropies as observed in our work.

In summary, we have observed a strong dependence of the proton energy spectra on the nature of the final high spin states belonging to different rotational bands in $^{82}$Sr, which cannot be accounted for in terms of phase-space effects. The large shifts toward lower energies and the stronger anisotropies when subbarrier protons lead to high spin states in the yrast band compared to the ground band are interpreted as due to near-yrast emission of high-$\ell$ protons. These results suggest that spectra and angular distributions of subbarrier protons may provide a sensitive probe of the structure of excited, rapidly-rotating nuclei.

The work described here was performed in collaboration with V. Abenante, J. R. Beene, Y. S. Chen, L. Courtney, G. Garcia-Bermudez, M. C. Griffin, M. L. Halbert, D. C. Hensley, N. R. Johnson, A. J. Larabee, G. A. Leander, I. Y. Lee , Z. Majka, F. K. McGowan, N. G. Nicolis, L. L. Riedinger, M. A. Riley, D. G. Sarantites, T. M. Semkow, D. W. Stacener, A. Virtanen, and J. Y. Zhang. Oak Ridge National Laboratory is operated by Martin Marietta Energy Systems, Inc. for the U.S. Department of Energy under contract No. DE-AC05-84OR21400.

## References

1. M. Jääskeläinen *et al.*, Nucl. Instr. Meth., **204**, 385 (1983).
2. C. Baktash *et al.*, Phys. Rev. Lett. **54**, 978 (1985).
3. I. Ragnarsson *et al.*, Phys. Rev. Lett. **54**, 982 (1985).
4. R. V. F. Janssens *et al.*, Phys. Lett. **152B**, 167 (1985).
5. M. A. Deleplanque *et al.*, Phys. Rev. Lett. **43**, 1001 (1979).
6. P. Chowdhury *et al.*, Phys. Rev. Lett. **47**, 778 (1981).
7. M. Jääskeläinen *et al.*, Phys. Lett. **119B**, 65 (1982).
8. P. M. Stwertka *et al.*, Phys. Rev. Lett. **54**, 1635 (1985); T. M. Cormier *et al.*, Phys. Rev. C **30**, 1953 (1984).
9. G. Bogaert *et al.*, Z. Phys. A **324**, 107 (1986); J. P. Thibaud *et al.*, Z. Phys. A **321**, 275 (1985)
10. Y. S. Chen and I. Hamamoto, Phys. Scr. **24**, 763 (1981).
11. Y. S. Chen and G. A. Leander, Phys. Rev. C **26**, 2607 (1982), and references therein.

12. J. Dudek and W. Nazarewicz, Phys. Rev. C **31**, 298 (1985).

13. A. L. Goodman, Phys. Rev. C **38**, 1092 (1988).

14. A. L. Goodman, Phys. Rev. C **39**, 2008 (1988).

15. A. L. Goodman, Phys. Rev. C **39**, 2478 (1988).

16. J. L. Egido and H. A. Weidenmüller, Phys. Lett. **208B**, 58 (1988); J. L. Egido and H. A. Weidenmüller, Phys. Rev. C **39**, 2398 (1989).

17. M. Blann and T.T. Komoto, Phys. Scr. **24**, 93 (1981).

18. J.M. Alexander, D. Guerreau and L.C. Vaz, Z. Phys. A **305**, 313 (1982).

19. Z. Majka *et al.*, Phys. Rev. Lett. **59**, 322 (1987).

20. J.B. Natowitz, Nucl. Phys. A **482**, 171c (1988).

21. F.A. Dilmanian *et al.*, Phys. Rev. Lett. **49**, 1909 (1982).

22. N.G. Nicolis *et al.* (to be published in Phys. Rev. C); and D.G. Sarantites *et al.* in *Spectroscopy of Heavy Nuclei* ed. J. Sharpey-Schafer (World Scientific, 1989, in press).

23. W. Nazarewicz *et al.*, Nucl. Phys. A **345**, 397 (1985), and private communication.

24. A CsI(Tℓ) version of the Dwarf Ball system described in: D.G. Sarantites *et al.*, Nucl. Instr. Meth. A **264**, 319 (1987).

25. C. Baktash *et al.*, B.A.P.S. **33**, 1585 (1988) (to be published).

26. A. Gavron, Phys. Rev. C **21**, 230 (1980); modification PACE2S by J.R. Beene (unpublished).

27. T. Døssing *et al.*, Nucl. Phys. A **287**, 137 (1977).